Dalton Transactions

PAPER

View Article Online
View Journal | View Issue

Cite this: *Dalton Trans.*, 2017, **46**, 16983

All-gas-phase synthesis of amino-functionalized UiO-66 thin films†

Kristian Blindheim Lausund, *[a,b] Veljko Petrovic[a,b] and Ola Nilsen *[a,b]

Thin films of metal–organic frameworks (MOFs) prepared using all-gas-phase techniques such as atomic/molecular layer deposition (ALD/MLD) are emerging due to their potential for enabling suitable applications. Their high and specific porosity enables their use as membranes for separations and as a basis for sensors in microelectronics, provided that films can be made. The properties of such MOF materials can be tuned by choosing linker molecules that are functionalized with a variety of chemical groups. However, thin films of these functionalised MOFs have so far been prepared through wet based chemistries, which are difficult to combine with microelectronics and high aspect ratio structures. We here report on the thin film deposition of amino-functionalised UiO-66 through an all-gas-phase ALD/MLD process. By using amino-functionalised linkers, modulation by acetic acid to control the stoichiometry of the deposited film was no longer required, as opposed to the case in which unmodified terephthalic acid was used as a linker. The growth and properties of the films were characterised using an *in situ* quartz crystal microbalance (QCM), spectroscopic ellipsometry (SE), grazing incidence X-ray diffraction (GIXRD), Fourier transform infrared spectroscopy (FTIR) and other techniques to obtain information on their growth dynamics and physical properties.

Received 19th September 2017,
Accepted 25th October 2017

DOI: 10.1039/c7dt03518g

rsc.li/dalton

Introduction

Metal–organic frameworks (MOFs) are a class of materials that consists of inorganic metal-based clusters bound together by organic linker molecules. This creates a highly ordered porous framework with well-defined pore sizes with narrow distributions.[2] The porosity of these materials exceeds that of the well-known zeolites, making them attractive for several applications such as gas storage,[3] catalysis,[4] separations,[5] drug delivery,[6] handling and destruction of toxins,[7–9] and degradation of chemical warfare agents.[9,10] So far, the majority of these MOF materials have only been produced as powders through wet based techniques such as solvothermal synthesis. By enabling the deposition of such materials as thin films, crystalline or amorphous, numerous new areas of applications such as membrane filters and integrated sensors or low-κ dielectrics in microelectronics can be realised.[11]

The properties of MOFs can be tuned to serve different needs by functionalising the linker molecule itself. Among the properties that are demonstrated to be tunable are selectivity to certain gas molecules,[12,13] hydrophilicity,[14] and catalytic properties.[15] It is thus also of interest to investigate how the functionalisation of the linkers affects the growth of such materials. In this study we compare the growth of UiO-66 with amino-functionalised terephthalic acid (UiO-66-NH_2) with our prior reports on the deposition of UiO-66 using terephthalic acid.[1]

The atomic layer deposition (ALD) technique, also known as molecular layer deposition (MLD)[16–18] when larger molecules are included in the growth, such as here, enables the outmost control of the deposited material even when deposited on complex geometries. The film is made one atomic or molecular layer at a time through gas-to-surface reactions. The precursors are pulsed sequentially and separately into the reaction chamber where they react with and saturate the surfaces of the substrates. Inert gas purge steps separate the precursor pulses and avoid reactions in the gas phase. By repeating these steps for a given number of cycles, a thin film with the desired thickness is made. A more thorough description of the deposition technique is given in the reviews.[19–21]

By enabling the thin film deposition of functionalized MOFs through MLD, we can introduce the same tunability as noticed in traditionally synthesized MOFs for applications in which an all-gas-phase deposition technique is required, such as in microelectronics.

[a]*Department of Chemistry, University of Oslo, Postboks 1033, Blindern, 0315 OSLO, Norway. E-mail: ola.nilsen@kjemi.uio.no, k.b.lausund@kjemi.uio.no*
[b]*Centre for Materials Science and Nanotechnology, University of Oslo, Postboks 1033, Blindern, 0315 OSLO, Norway*

†Electronic supplementary information (ESI) available: Some additional results including TG data for the organic precursor (2-amino-1,4-BDC), GIXRD diffractograms for post-treated films that were deposited at 315 °C and a graph showing the full porosity test. See DOI: 10.1039/c7dt03518g

Another important factor that affects the applicability of MOF thin films is their stability. In the early days of MOF-research, the crystals were unstable when removed from the solution in which they were made. Numerous examples of stable MOF-compounds have now been demonstrated, and it is important to choose the appropriate one among these when designing for applications.[22] Our choice has been the thermally and chemically stable UiO-66 type as the basis for further explorations.[23]

There are only few examples in the literature of MOF thin films with functional groups on the linkers, and no examples where the films are made by all-gas phase processes such as MLD. These films are typically made by liquid phase epitaxial growth (LPE) on self-assembled monolayers (SAMs) on gold substrates. One example is the work performed by Shekhah *et al.*[24] who used LPE on a SAM functionalized gold surface to make a layer based MOF with the chemical formula $[Cu_2(NH_2\text{-bdc})_2(dabco)]$ where NH_2-bdc = 2-amino-1,4-benzene dicarboxylic acid (abbreviated in this work as 2-amino-1,4-BDC), and dabco = 1,4-diazabicyclo[2.2.2]octane. They also demonstrated the possibility of post-synthesis modification (PSM) by allowing the NH_2 groups to react with larger chemical groups such as 1-ferrocenylmethylisocyanate. Another example of functionalized MOF thin films made by this technique is the work by Wang *et al.*[25] where they made $[Zn_2(N_3\text{-bdc})_2(dabco)]$ (N_3-bdc = 2-azidoterephthalic acid) and demonstrated PSM by reactions with the azido group. An example of functionalized MOF films that are synthesized through a different approach is seen in the work by Yoo *et al.*[26] in which a film of IRMOF-3 (amino-functionalized) is grown by solvothermal synthesis on a surface seeded by IRMOF-1 (non-functionalized) crystals.

Our present films are made using $ZrCl_4$ and 2-amino-1,4-benzene dicarboxylic acid (2-amino-1,4-BDC, also known as 2-amino-terephthalic acid) and will be compared to our prior work on the deposition of UiO-66 using $ZrCl_4$ and 1,4-benzene dicarboxylic acid (1,4-BDC, also known as terephthalic acid).[1]

Experimental

Atomic/molecular layer deposition

The ALD/MLD depositions were performed in an F-120 Sat-type ALD reactor (ASM Microchemistry Ltd) using $ZrCl_4$ (MERCK Schuchardt OHG >98%) and 2-amino-1,4-benzene dicarboxylic acid (2-amino-1,4-BDC) (Sigma-Aldrich 99%) as precursors. Acetic acid (MERCK KGaA 100%) was also used as a co-reactant in selected experiments. The carrier and purging gas was N_2 (AGA 99.999%). A total flow of *ca.* 250 sccm (standard cubic centimetres per minute) of N_2 was used throughout the experiments, leading to a background pressure of *ca.* 5 mBar. The vaporization temperatures for $ZrCl_4$ and 2-amino-1,4-BDC were set to 165 and 225 °C, respectively, based on previous work[17] and TG results that were collected using a NETZSCH 209 F1 Libra with a Pt/Rh stage and a type S thermocouple with a dry aluminium crucible. Acetic acid was kept at room temperature in an external container. The films were deposited on as-received, pre-cleaned Si(001) substrates of 2 × 2 cm^2. Their native oxide thickness was measured by spectroscopic ellipsometry (SE) before deposition and taken into account when the film thickness was determined.

In situ quartz crystal microbalance (QCM)

In situ QCM analyses were conducted using two 6 MHz AT cut quartz crystals mounted *ca.* 5 cm apart on a home-made holder in order to monitor the mass increase during the deposition and uncover possible delayed saturations through the reaction chamber. The signals were recorded using a Maxtek TM-400 and processed by averaging over 16 consecutive cycles. The signal from the QCM analysis was converted from $-\Delta$ Hz to ng cm^{-2} by calibrating the sensitivity of each sensor with the thickness and density data obtained by XRR of films deposited separately from the QCM measurements. Variations in sensitivity of the sensors throughout the QCM experiment were also corrected for by using a standard sequence repeatedly throughout the experiment and adjusting all results based on variations in this standard. In order to ensure a reliable response from the QCM-crystals, the temperature was stabilised for 3 hours before any experiments were conducted. This setup was also used for a porosity test where the QCM detectors were used to measure the amount of water that was adsorbed in the porous films.

Post-deposition treatment

Some of the films were exposed to moisture for 24 h in a chamber that was held at a relative humidity of 70–75% by storing a saturated NaCl solution in the chamber to investigate the effect of moisture on the films. The crystallization of the films was performed by heating the samples to 160 °C for 24 h in a sealed autoclave with an internal volume of 35 ml. This was done with dry or moist air and with or without adding approximately 0.1 ml of acetic acid in the autoclave. Crystallization occurred only when acetic acid was added.

Characterisation of the films

The thickness and the refractive index of each film were measured using spectroscopic ellipsometry. SE data were collected using a J. A. Woollam alpha-SE spectroscopic ellipsometer employing a wavelength range of 390–900 nm, and modelled to a Cauchy-function using the CompleteEASE software package in order to determine the thicknesses and refractive indices (at λ = 632.8 nm) of the films. Grazing incidence X-ray diffraction (GIXRD) and X-ray reflectivity (XRR) analyses were performed using a PANalytical Empyrean diffractometer, equipped with a Cu Kα source powered at 45 kV/40 mA (λ = 1.5406 Å), a parallel beam X-ray mirror and a proportional point detector (PW 3011/20). For GIXRD the incident angle was ω = 0.30° while for XRR analysis 2θ was scanned from 0.08° to 6°. The XRR results were analysed using the X'Pert Reflectivity software provided by PANalytical. Fourier transform infrared (FTIR) spectroscopy was for the most part performed using a Bruker VERTEX 70 FTIR spectrometer in the transmission mode. An exemption was the as-deposited samples for which the spectra were collected using a Cary 630

FT-IR in the transmission mode. A spectrum obtained from an uncoated silicon substrate was used as the background. Scanning electron microscopy (SEM) images were obtained using a HITACHI SU8230 scanning electron microscope with a cold cathode field emission type electron gun. The working distance was approximately 2 mm, and the acceleration voltage was typically 1 kV with a beam current of 10 μA.

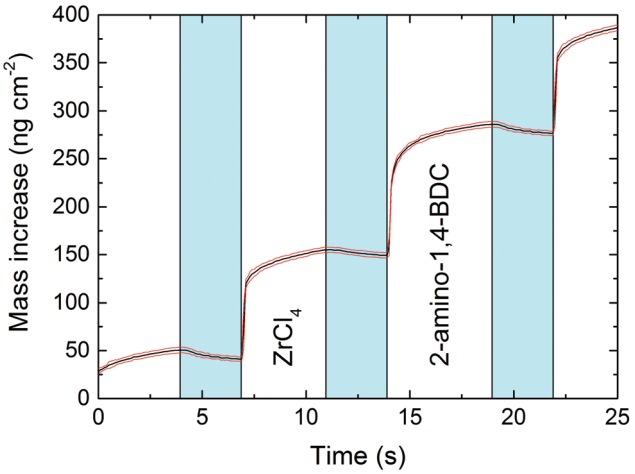

Fig. 1 Quartz crystal microbalance characterization. Mass gain as a function of time measured *in situ* in the molecular layer deposition (MLD) process with quartz crystal microbalance (QCM) while alternating between $ZrCl_4$ and 2-amino-terephthalic acid (2-amino-1,4-BDC) pulses separated by inert gas (N_2) purges (blue). The red lines show the standard deviations for the QCM data (n = 16).

Results

Thermogravimetric (TG) analysis was performed on the 2-amino-1,4-BDC precursor to aid in determining a suitable precursor temperature (ESI Fig. 1†). This, combined with the visual inspection of the precursor during heating, showed a suitable precursor temperature of *ca.* 225 °C. The deposition was investigated using an *in situ* quartz crystal microbalance (QCM) for deposition at a reactor temperature of 265 °C using a pulsing sequence of 4 s $ZrCl_4$, 3 s purge, 5 s 2-amino-1,4-BDC, and 3 s purge (hereafter termed 4-3-5-3), Fig. 1. Both precursors show self-limiting growth (Fig. 2).

The growth rate as a function of pulse and purge lengths was investigated by varying one parameter individually while keeping the others constant at 4-3-5-3, Fig. 2. This experiment was performed using two QCM detectors situated 5 cm apart along the flow direction in the deposition chamber, and the experiment was repeated two times for the investigation of the pulse lengths.

The reactions show a self-saturating behaviour with full saturation after 4 s for both precursors. It is possible to observe a delayed response in the QCM signal for the sensor situated in the back of the reaction chamber. This indicates that the

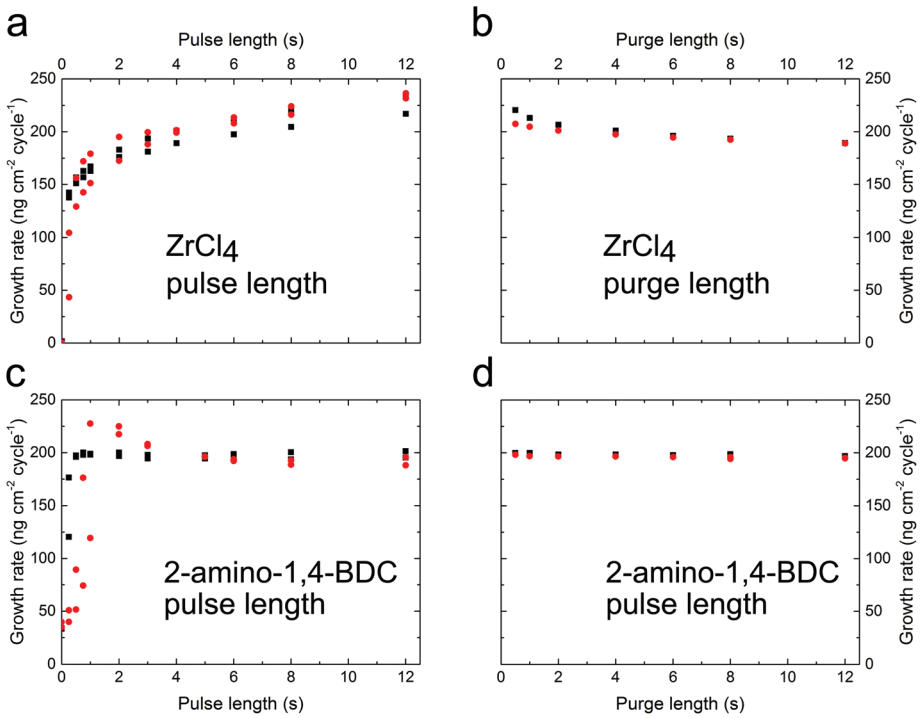

Fig. 2 Test of self-saturating growth. The growth rates for the ALD/MLD system measured using a QCM with a basic pulsing sequence of 4 s $ZrCl_4$, 3 s purge, 5 s 2-amino-1,4-BDC, and 3 s purge (termed in the text as 4-3-5-3) while the parameters were varied individually. The parameters that are varied are (a) the $ZrCl_4$ pulse length, (b) the $ZrCl_4$ purge length, (c) the 2-amino-1,4-BDC pulse length and (d) the 2-amino-1,4-BDC purge length. Two sensors were used, one in the front of the reaction chamber (black squares) and one in the back (red circles). The pulse length experiments were performed two times.

surface reactions are fast and complete so that almost no precursor reaches the back of the reaction chamber until the front of the chamber is fully saturated.

The dependency of the deposition temperature on the growth rate was investigated using 100 cycles as the standard, Fig. 3. The growth rate decreases with increasing deposition temperature from 10 Å per cycle at 240 °C to 7.5 Å per cycle at 390 °C while the refractive index increases slightly in the same range. For comparison, the index of refraction of ZrO_2 is 2.16.

Previously, we have shown that films deposited with 1,4-BDC (without amino-functionalization) in the same manner as above contained an excess of this linker molecule that would crystallize on the surface of the film when exposed to a relative humidity of 70–75% over 24 h. The origin of this excess amount of linker was the monodentate coordination of a selection of linkers with the Zr-atoms. A fully bidentate coordination could be achieved by adding a pulse of acetic acid in the deposition process. The acetic acid functioned as a modulator that released the monodentate 1,4-BDC leaving only the desired linkers with a bidentate coordination. However, when functionalized 2-amino-1,4-BDC is used, the steric hindrance from the amino group ensures that the linkers coordinate in the correct, bidentate manner without a need for further modulation, as illustrated in Fig. 4. This is also seen throughout our results, for instance, after exposure to humid air, we see no evidence of crystallisation of the excess linker from grazing incidence X-ray diffraction (GIXRD) analysis or the development of surface roughness, Fig. 5b. We also see from the QCM experiments that the acetic acid that is pulsed in addition to $ZrCl_4$ and 2-amino-1,4-BDC does not lead to any overall change in the mass during exposure and purge, nor does it alter the mass ratio between $ZrCl_4$ and 2-amino-1,4-BDC, Fig. 5a. Finally, the density of the films as determined by X-ray reflectivity (XRR) is unaffected by the added acetic acid pulse whereas the density increased when modulation was introduced in the system where regular 1,4-BDC was used.

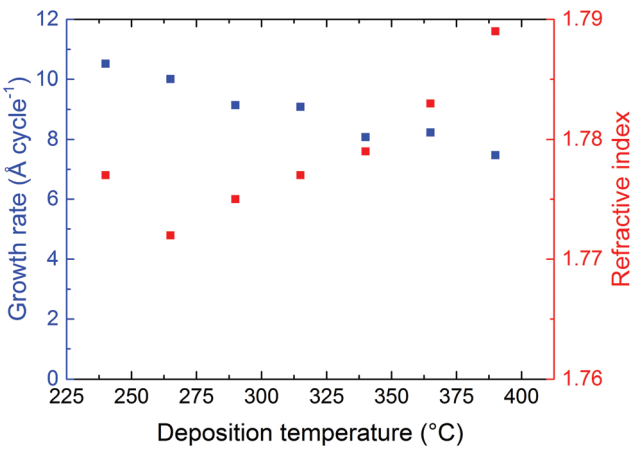

Fig. 3 Varying the deposition temperature. The growth rate of the ALD/MLD system and the refractive index of the films as a function of the deposition temperature.

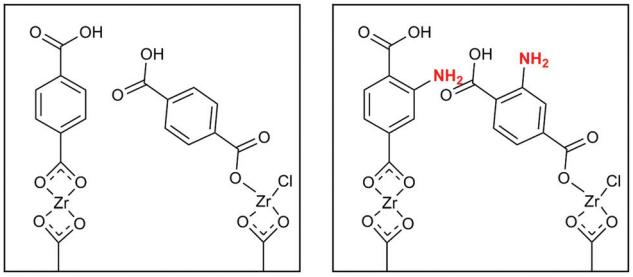

Fig. 4 Steric hindrance. An illustration of monodentate and bidentate coordination of un-functionalized 1,4-BDC (left) compared to the amino-functionalized 2-amino-1,4-BDC (right) that coordinates only in a bidentate due to steric hindrance.

All further samples were deposited without acetic acid modulation. The crystallization of the films was performed in the same manner as described in our previous work, by placing the coated substrates in a sealed autoclave along with approximately 0.1 ml of acetic acid and heating to 160 °C for 24 hours.

There is still a possibility that the moisture in ambient air can affect the crystallisation process. In order to better understand the importance of acetic acid compared to that of humid air in the crystallisation, we treated four samples deposited with 500 cycles at 265 °C in sealed autoclaves with and without acetic acid after exposing the samples to either dry or humid air. It is clear from the GIXRD diffractograms in Fig. 6 that crystallisation occurs only in the presence of acetic acid. The importance of the humidity in air is less clear as it is difficult to completely prevent exposure to humidity when acetic acid is also used. The effect of humidity is therefore not conclusive. The same test was done for four samples deposited with 500 cycles at 315 °C. This resulted in no crystallinity in any of the samples, indicating that a very high deposition temperature prevents crystallization into any MOF structure (ESI Fig. 2†). FTIR analysis (not shown) of these films shows significant changes in the peaks corresponding to the amino group in 2-amino-1,4-BDC. These changes may indicate partial decomposition or polymerisation of the linkers under these deposition conditions.

The crystallisation of the films resulted in numerous crystallites forming on the surface, as can be seen in the scanning electron microscope (SEM) images in Fig. 7. Some of these crystallites are hexagonally shaped, which does not cohere with the regular cubic crystal structure for UiO-66. We therefore assume that the present film rather crystallises in a layered type of UiO-66 similar to the one described by Cliffe *et al.*[27] The hexagonal shape of the crystallites is even more pronounced in the SEM images in Fig. 8.

Fourier transform infrared (FTIR) spectroscopy was used to determine the coordination of the carboxylate group with the Zr atoms as well as to confirm that the amino group is present in the final product. The amount of splitting between the peaks corresponding to the symmetric and asymmetric stretch of the carboxylate group indicates the coordination to the metal atoms. A bidentate coordination has a splitting of 50–150 cm^{-1}, which is seen for the amorphous samples that were autoclave

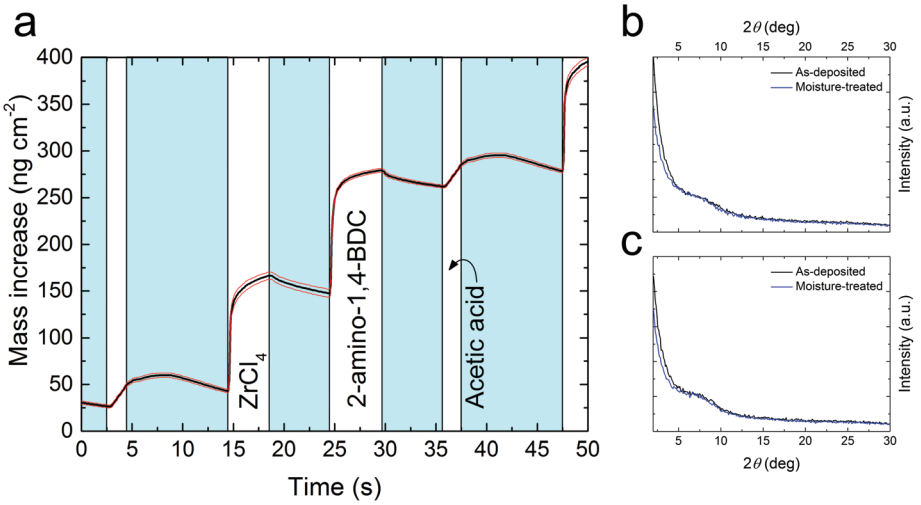

Fig. 5 Effects of acetic acid modulation on the ALD process. (a) QCM measurements of an ALD/MLD process in which a modulation step with acetic acid is included. The blue panels indicate the purge steps. The red lines show the standard deviation (n = 16). (b) and (c) Grazing incidence X-ray diffraction (GIXRD) diffractograms of samples deposited without and with acetic acid modulation, respectively, before (black) and after (blue) exposure to moist air (70–75% relative humidity for 24 h).

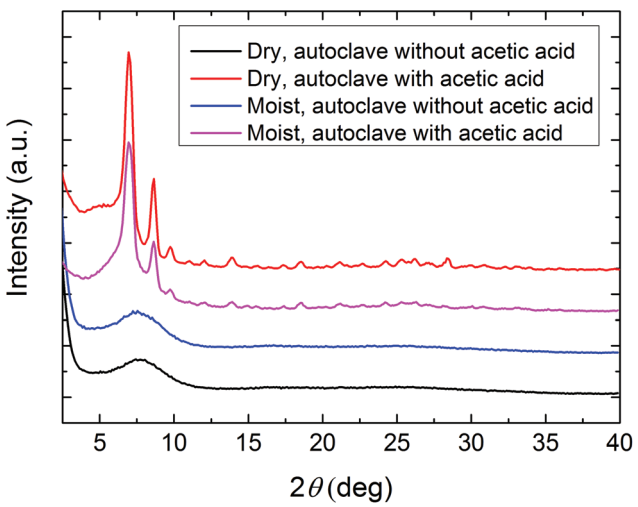

Fig. 6 Post-deposition autoclave treatment. GIXRD diffractograms for four samples that were treated in an autoclave with (magenta, red) or without (black, blue) acetic acid after being exposed to dry (black, red) or moist (blue, magenta) air after the deposition.

treated without acetic acid. A bridging coordination gives a splitting of 130–200 cm^{-1}. This is seen for the crystalline samples that were autoclave treated with acetic acid. A monodentate coordination would give a larger splitting than 200 cm^{-1}. This is not seen in any of the autoclave treated samples (Fig. 9a) or in the as-deposited samples with or without acetic acid modulation (Fig. 9b), again, indicating that the steric hindrance from the amino group prevents an excess amount of 2-amino-1,4-BDC to form a monodentate coordination with Zr.

In all of these spectra we see a peak at approximately 1260 cm^{-1} corresponding to the C–N stretch of the amino group, and a set of twin peaks between 3350 and 3500 cm^{-1} corresponding to the N–H stretches of the amino group. In the crystalline films that have been autoclave treated with acetic acid the peaks corresponding to the N–H-stretch are partly concealed by a broad water-peak, indicating that a lot of water is adsorbed in the pores of these films. Fig. 9c shows a cut-out of the N–H stretch.

In order to determine the porous nature of the films, a porosity test was performed in the same manner as in our prior work for UiO-66,[1] Fig. 10. This was performed by measuring the water uptake during a water pulse in the ALD-reactor at room temperature on two coated QCM crystals where one film was crystallized and the other was left amorphous. The pulse lengths that were used were first 5 seconds and then 2 minutes of exposure, followed by long purge steps where most (but not all) of the water was removed. After the five-second pulse, the film was not fully saturated with water unlike the un-functionalized UiO-66 film. The remaining water after the first pulse and purge was removed by heating to 150 °C for approximately 2 hours followed by a 24-hour-long temperature stabilization, leaving the water content slightly lower than the initial value, indicating that there was a small amount of water in the structure before the five-second pulse. The full experiment is shown in ESI Fig. 3.† This indicates that water adsorbs more strongly to these films than to the regular UiO-66 films without amino-functionalization. We also see that it takes a longer time for these films to be fully saturated with water than that for the films with non-functionalized 1,4-BDC. This could be due to a combination of increased adsorption to the amino group and reduction in the pore size where the amino–water complex slows down the diffusion of subsequent water molecules entering the film. Both the amorphous and the crystalline films are porous and have a much larger water uptake than the uncoated crystals (inset in Fig. 10), and the crystallisation process almost doubles the porosity.

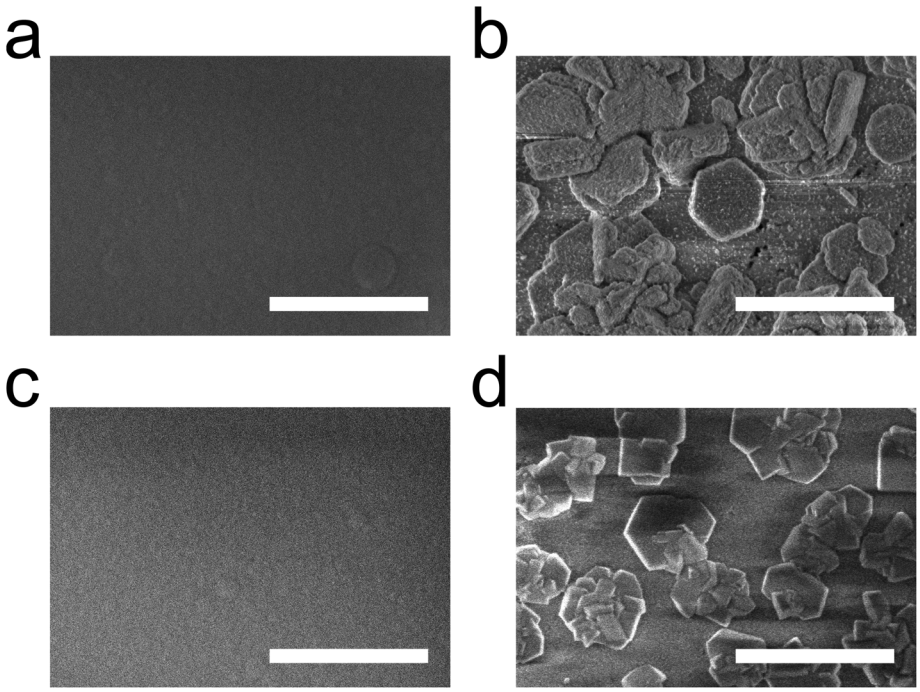

Fig. 7 Scanning electron microscopy. SEM images of four samples that were exposed to either dry or moist air and were treated in an autoclave after deposition: (a) exposed to dry air and autoclave treated without acetic acid, (b) exposed to dry air and autoclave treated with acetic acid, (c) exposed to moist air and autoclave treated without acetic acid, and (d) exposed to moist air and autoclave treated with acetic acid. All the scale bars are 1 μm long.

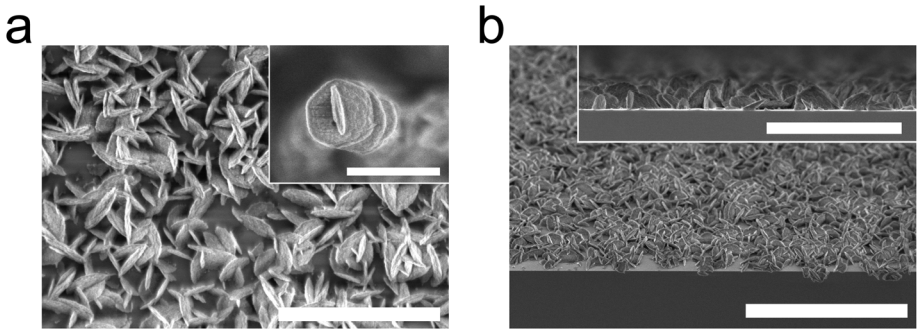

Fig. 8 Scanning electron microscopy. SEM images of a sample that was deposited with 100 cycles and crystallized in an autoclave with acetic acid and ambient air. (a) A top down view with an enlarged image of a hexagonal crystallite in the inset; the scale bars are 2 and 1 μm respectively. (b) A cross section view at a 45° angle with a cross section view at a 90° angle in the inset; the scale bars are 5 and 2 μm respectively.

The amino-functionalization of the linker alters some of the properties of the film. The hydrophilicity is increased as compared to that of un-functionalised UiO-66 films, as measured by its contact angle towards water, Fig. 11. Both of the films are in the amorphous as-deposited state.

Discussion

The MLD system in which $ZrCl_4$ and 2-amino-1,4-BDC were used as precursors shows self-terminating growth of each precursor, as measured by *in situ* QCM (Fig. 1, 2 and 5a). The growth rate is close to 1 nm per cycle for depositions at 265 °C, which is higher than that observed in the un-functionalized UiO-66 films.[1] This is notably higher than those with regular ALD processes, but within reach of many MLD systems (Fig. 3). One possible reason for the high growth rate is that the carboxylate groups in this case always coordinate in a bidentate manner causing the 2-amino-1,4-BDC molecules to be aligned normal to the substrate instead of being at an angle similar to that of the carboxylate groups with a monodentate coordination.

The growth rate decreases with increasing deposition temperatures indicating that the precursors desorb from the surface at higher temperatures, or cause disordered growth due to

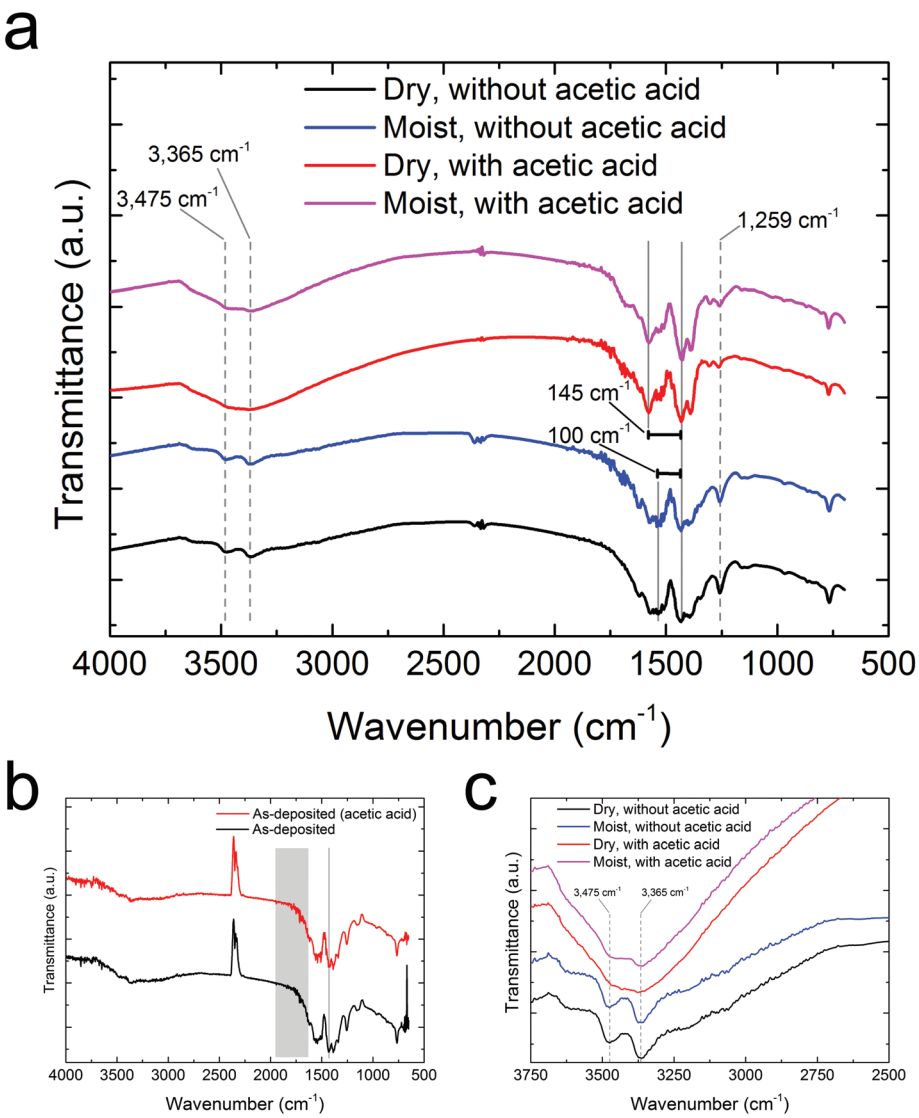

Fig. 9 Fourier transform infrared spectroscopy. (a) The full FTIR spectra for four samples that were treated in an autoclave with (magenta, red) or without (black, blue) acetic acid after being exposed to dry (black, red) or moist (blue, magenta) air after the deposition. (b) The FTIR spectra for two as-deposited samples that were deposited with (red) or without (black) acetic acid modulation. The grey box marks the area with a larger splitting than 200 cm^{-1} from the main peak (grey line), which is where a peak corresponding to monodentate coordination would be. (c) An enlarged view of the N–H stretch peaks from the amino group and the O–H stretch peaks from water for the same samples as in (a). Solid lines indicate carboxylate group peaks and dashed lines indicate amino group peaks.

increased entropy. In addition to this, it is probable that the organic precursor decomposes and/or polymerizes at high temperatures, which prevents the crystallization of films deposited at a very high temperature.

A comparison of the QCM results of Fig. 1 and 5a shows that the mass responses for the $ZrCl_4$ and 2-amino-1,4-BDC are virtually unaffected by the acetic acid pulse, with respect to both relative responses ($\Delta m(ZrCl_4$ pulse$) : \Delta m$(2-amino-1,4-BDC) = 0.85) and their absolute values in ng cm^{-2}.

As with the growth of the unmodified UiO-66 material, it is possible to postulate two overall reaction mechanisms, leading to a Zr : 2-amino-1,4-BDC stoichiometry of 1 : 2 or 1 : 1, where the latter is expected for the UiO-66 structure type.

1 : 2 stoichiometry:
$ZrCl_4$ pulse:

$$|\text{–}(OH)_x + ZrCl_4(g) = |\text{–}(O)_xZrCl_{(4-x)} + xHCl$$

2-Amino-1,4-BDC pulse:

$$|\text{–}(O)_xZrCl_{(4-x)} + 2 \times \text{2-amino-1, 4-BDC(g)} = |\text{–}(O)_xZr(\text{2-amino-1, 4-BDC})_2 + (4-x)HCl$$

where $x = 0.75$ results in the observed relative mass increase of ($\Delta m(ZrCl_4$ pulse$) : \Delta m$(2-amino-1,4-BDC) = 0.85. This is somewhat lower than that practically possible, since it assumes that

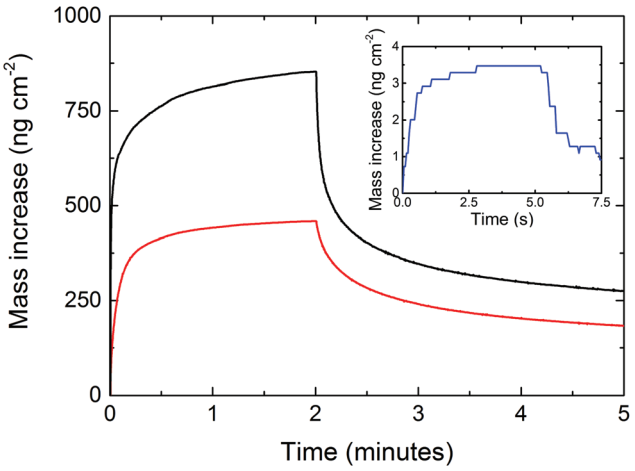

Fig. 10 Porosity test. The water uptake in an as-deposited, amorphous film (black) and a post-deposition treated, crystalline film (red) as a function of time for a 2 minute long water pulse in the ALD reactor at room temperature, as measured by QCM. The inset shows the water uptake on an uncoated QCM-crystal during a 5 second water pulse as a control.

25% of the $ZrCl_4$ molecules are physisorbed rather than chemisorbed so that HCl is not lost from the surface.

1 : 1 stoichiometry:

$ZrCl_4$ pulse:

$$|\text{–}(OH)_x + ZrCl_4(g) = |\text{–}(O)_xZrCl_{(4-x)} + x\text{HCl}$$

2-Amino-1,4-BDC pulse:

$$|\text{–}(O)_xZrCl_{(4-x)} + \text{2-amino-1,4-BDC}(g) = |\text{–}(O)_xZr(\text{2-amino-1,4-BDC}) + (4-x)\text{HCl}$$

where x = 3.0 results in the observed relative mass increase of (Δm($ZrCl_4$ pulse) : Δm(2-amino-1,4-BDC) = 0.85. This is within the expected range of x = 1–3 for reactions with $ZrCl_4$ as a precursor, and indicate that $ZrCl_4$ is highly reactive during the growth.

In our previous work,[1] an acetic acid modulation was required in order to achieve the correct stoichiometry between the metal atoms (Zr) and the organic linkers (1,4-BDC). This is not necessary when 2-amino-1,4-BDC is used as the linker, as can be seen from several of our results. First, there is no excess of the linker molecules crystallizing on the surface of films that have been exposed to moisture, causing the GIXRD diffractograms for films deposited with and without acetic acid modulation to be more or less identical (Fig. 5b and c). The QCM results also show that the overall reaction scheme is virtually unaffected by acetic acid. This also applies to the density as measured by XRR and FTIR analyses. From the FTIR analysis there is also no sign of monodentate coordination of the carboxylate group with the Zr atoms, which is the coordination mode of the excess linkers in our previous work mentioned above.

One possible explanation for modulation not being required for the amino-functionalized linker is that the steric hindrance of the amino group in a bidentate linker prevents its neighbours to coordinate in an angled monodentate manner, causing all linkers to form a bidentate coordination (Fig. 4).

From the GIXRD diffractograms in Fig. 5b and c (and the FTIR spectra in Fig. 9b) it is clear that the as-deposited films are amorphous both with and without acetic acid modulation. The films can, however, be crystallised through heating in a sealed autoclave with a small amount of acetic acid as seen from the GIXRD diffractograms in Fig. 6 (and the FTIR spectra in Fig. 9a).

In summary, we were able to prepare a crystalline, amino-functionalized MOF thin film through MLD. This amino-functionalization alters the properties of the film such as the heat of adsorption of water in the pores and can make it suitable for different applications than the un-functionalized MOF. The fact that thin films of this functionalized MOF can be made through ALD may enable it to be used in microelectronics such as sensors where normal solvothermal synthesis cannot be used due to the stiction of small components. The amino group also facilitates a more simple deposition process in that the acetic acid modulation is no longer required.

Conclusion

Thin films of crystalline, amino-functionalized UiO-66 (UiO-66-NH_2) were made by depositing a thin film by MLD, using 2-amino-1,4-BDC and $ZrCl_4$ as precursors, followed by post-deposition crystallisation. The amino-functionalization proved to be an advantage in the deposition process by eliminating the need for an acetic acid modulation step. The films

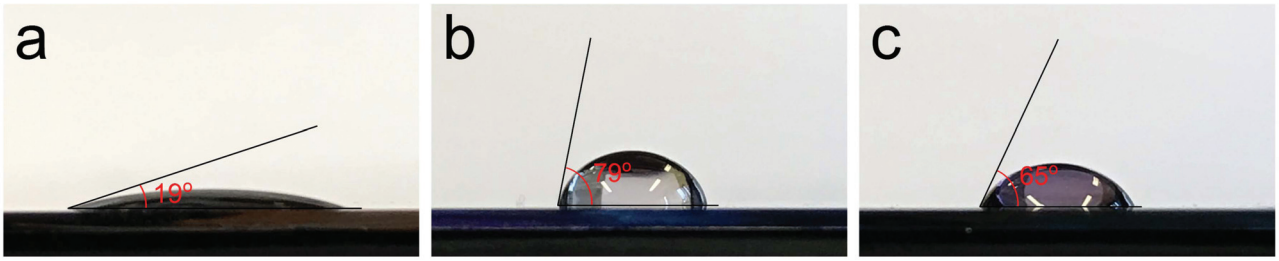

Fig. 11 Contact angle measurements. The contact angle of water on (a) a clean substrate, (b) an as-deposited, amorphous UiO-66 film (not amino-functionalized), and (c) an as-deposited, amorphous, amino-functionalized UiO-66-NH_2 film.

were characterized before and after crystallization using GIXRD, FTIR and SEM, all of which indicate that the crystallization was successful. Contact angle measurements and porosity measurements were also conducted, and they show that UiO-66-NH_2 has some different properties compared with the un-functionalized UiO-66 such as a more hydrophilic character.

Conflicts of interest

There are no conflicts to declare.

Acknowledgements

We thank the strategic research initiative Diatech@UiO at the University of Oslo for funding. K. B. L. is also thankful to the co-supervisors of this project Elsa Lundanes, Carl Henrik Gørbitz and Steven Wilson for their ideas and comments; Sigurd Øien-Ødegaard and Fredrik Lundvall for discussions regarding crystal structures; Leva Momtazi for FTIR measurements and discussions; Asbjørn Slagtern Fjellvåg for TG measurements; and to other colleagues at the University of Oslo for their aid. We also like to thank the Norwegian national infrastructure for X-ray diffraction and scattering (RECX), and the Department of Geosciences at the University of Oslo for use of the X-ray fluorescence equipment.

References

1 K. B. Lausund and O. Nilsen, All-gas-phase synthesis of UiO-66 through modulated atomic layer deposition, *Nat. Commun.*, 2016, **7**, 13578.
2 H. Li, M. Eddaoudi, M. O'Keeffe and O. M. Yaghi, Design and synthesis of an exceptionally stable and highly porous metal-organic framework, *Nature*, 1999, **402**(6759), 276–279.
3 H. R. Abid, H. Tian, H.-M. Ang, M. O. Tade, C. E. Buckley and S. Wang, Nanosize Zr-metal organic framework (UiO-66) for hydrogen and carbon dioxide storage, *Chem. Eng. J.*, 2012, **187**, 415–420.
4 J. Lee, O. K. Farha, J. Roberts, K. A. Scheidt, S. T. Nguyen and J. T. Hupp, Metal-organic framework materials as catalysts, *Chem. Soc. Rev.*, 2009, **38**(5), 1450–1459.
5 X. Liu, N. Keser Demir, Z. Wu and K. Li, Highly Water Stable Zirconium Metal-Organic Framework UiO-66 Membranes Supported on Alumina Hollow Fibers for Desalination, *J. Am. Chem. Soc.*, 2015, **137**(22), 6999–7002.
6 K. M. L. Taylor-Pashow, J. D. Rocca, Z. Xie, S. Tran and W. Lin, Postsynthetic Modifications of Iron-Carboxylate Nanoscale Metal–Organic Frameworks for Imaging and Drug Delivery, *J. Am. Chem. Soc.*, 2009, **131**(40), 14261–14263.
7 S. Jakobsen, D. Gianolio, D. S. Wragg, M. H. Nilsen, H. Emerich, S. Bordiga, C. Lamberti, U. Olsbye, M. Tilset and K. P. Lillerud, Structural determination of a highly stable metal-organic framework with possible application to interim radioactive waste scavenging: Hf-UiO-66, *Phys. Rev. B: Condens. Matter*, 2012, **86**(12), 125429.
8 C. Wang, X. Liu, J. P. Chen and K. Li, Superior removal of arsenic from water with zirconium metal-organic framework UiO-66, *Sci. Rep.*, 2015, **5**, 16613.
9 J. E. Mondloch, M. J. Katz, W. C. Isley Iii, P. Ghosh, P. Liao, W. Bury, G. W. Wagner, M. G. Hall, J. B. DeCoste, G. W. Peterson, R. Q. Snurr, C. J. Cramer, J. T. Hupp and O. K. Farha, Destruction of chemical warfare agents using metal–organic frameworks, *Nat. Mater.*, 2015, **14**(5), 512–516.
10 D. T. Lee, J. Zhao, G. W. Peterson and G. N. Parsons, Catalytic "MOF-Cloth" Formed via Directed Supramolecular Assembly of UiO-66-NH2 Crystals on Atomic Layer Deposition-Coated Textiles for Rapid Degradation of Chemical Warfare Agent Simulants, *Chem. Mater.*, 2017, **29**(11), 4894–4903.
11 M. D. Allendorf, A. Schwartzberg, V. Stavila and A. A. Talin, A Roadmap to Implementing Metal–Organic Frameworks in Electronic Devices: Challenges and Critical Directions, *Chem. – Eur. J.*, 2011, **17**(41), 11372–11388.
12 P. Serra-Crespo, E. V. Ramos-Fernandez, J. Gascon and F. Kapteijn, Synthesis and Characterization of an Amino Functionalized MIL-101(Al): Separation and Catalytic Properties, *Chem. Mater.*, 2011, **23**(10), 2565–2572.
13 G. E. Cmarik, M. Kim, S. M. Cohen and K. S. Walton, Tuning the Adsorption Properties of UiO-66 via Ligand Functionalization, *Langmuir*, 2012, **28**(44), 15606–15613.
14 S.-N. Kim, J. Kim, H.-Y. Kim, H.-Y. Cho and W.-S. Ahn, Adsorption/catalytic properties of MIL-125 and NH2-MIL-125, *Catal. Today*, 2013, **204**, 85–93.
15 W. Kleist, M. Maciejewski and A. Baiker, MOF-5 based mixed-linker metal–organic frameworks: Synthesis, thermal stability and catalytic application, *Thermochim. Acta*, 2010, **499**(1), 71–78.
16 O. Nilsen, K. Klepper, H. Nielsen and H. Fjellvaåg, Deposition of organic-inorganic hybrid materials by atomic layer deposition, *ECS Trans.*, 2008, **16**(4), 3–14.
17 K. B. Klepper, O. Nilsen and H. Fjellvag, Deposition of thin films of organic-inorganic hybrid materials based on aromatic carboxylic acids by atomic layer deposition, *Dalton Trans.*, 2010, **39**(48), 11628–11635.
18 P. Sundberg and M. Karppinen, Organic and inorganic–organic thin film structures by molecular layer deposition: A review, *Beilstein J. Nanotechnol.*, 2014, **5**(1), 1104–1136.
19 V. Miikkulainen, M. Leskelä, M. Ritala and R. L. Puurunen, Crystallinity of inorganic films grown by atomic layer deposition: Overview and general trends, *J. Appl. Phys.*, 2013, **113**(2), 021301.
20 M. Leskelä, M. Ritala and O. Nilsen, Novel materials by atomic layer deposition and molecular layer deposition, *MRS Bull.*, 2011, **36**(11), 877–884.
21 X. Meng, An Overview of Molecular Layer Deposition for Organic and Organic-Inorganic Hybrid Materials: Mechanisms, Growth Characteristics, and Promising Applications, *J. Mater. Chem. A*, 2017, 18326–18378.

22 K. Leus, T. Bogaerts, J. De Decker, H. Depauw, K. Hendrickx, H. Vrielinck, V. Van Speybroeck and P. Van Der Voort, Systematic study of the chemical and hydrothermal stability of selected "stable" Metal Organic Frameworks, *Microporous Mesoporous Mater.*, 2016, **226**, 110–116.

23 J. H. Cavka, S. Jakobsen, U. Olsbye, N. Guillou, C. Lamberti, S. Bordiga and K. P. Lillerud, A new zirconium inorganic building brick forming metal organic frameworks with exceptional stability, *J. Am. Chem. Soc.*, 2008, **130**(42), 13850–13851.

24 O. Shekhah, H. K. Arslan, K. Chen, M. Schmittel, R. Maul, W. Wenzel and C. Wöll, Post-synthetic modification of epitaxially grown, highly oriented functionalized MOF thin films, *Chem. Commun.*, 2011, **47**(40), 11210–11212.

25 Z. Wang, J. Liu, H. K. Arslan, S. Grosjean, T. Hagendorn, H. Gliemann, S. Bräse and C. Wöll, Post-synthetic modification of metal–organic framework thin films using click chemistry: the importance of strained C–C triple bonds, *Langmuir*, 2013, **29**(51), 15958–15964.

26 Y. Yoo and H.-K. Jeong, Heteroepitaxial Growth of Isoreticular Metal– Organic Frameworks and Their Hybrid Films, *Cryst. Growth Des.*, 2010, **10**(3), 1283–1288.

27 M. J. Cliffe, E. Castillo-Martínez, Y. Wu, J. Lee, A. C. Forse, F. C. N. Firth, P. Z. Moghadam, D. Fairen-Jimenez, M. W. Gaultois, J. A. Hill, O. V. Magdysyuk, B. Slater, A. L. Goodwin and C. P. Grey, Metal–Organic Nanosheets Formed via Defect-Mediated Transformation of a Hafnium Metal–Organic Framework, *J. Am. Chem. Soc.*, 2017, **139**(15), 5397–5404.